NMR Study of the Distribution of Aromatic Molecules in NaY Zeolite

B. F. Chmelka, J. G. Pearson, S. B. Liu,† R. Ryoo,‡ L. C. de Menorval,§ and A. Pines*

Departments of Chemistry and Chemical Engineering, University of California—Berkeley, and Materials and Chemical Sciences Division, Lawrence Berkeley Laboratory, Berkeley, California 94720
(Received: June 7, 1990)

Local and macroscopic distributions of adsorbed benzene, 1,3,5-trimethylbenzene, and hexamethylbenzene (HMB) molecules among the intracrystalline cavities of NaY zeolite samples have been investigated by ^{129}Xe and multiple-quantum NMR. Xenon-129 NMR, a sensitive probe of macroscopic distributions of molecules in zeolites at room temperature, demonstrates the importance of sample heat treatment in distributing an adsorbate homogeneously throughout a collection of zeolite particles. NaY samples containing organic guests adsorbed at temperatures near the bulk species' melting point produce multiple or broad xenon lines characteristic of macroscopic (i.e., *inter*particle) adsorbate concentration gradients. After thorough heat treatment of the samples at elevated temperatures, the xenon spectrum collapses to a single sharp line, consistent with a macroscopically uniform distribution. For HMB adsorbed in NaY, "counting" hydrogen clusters by multiple-quantum NMR reveals *intra*particle HMB distributions consistent with one molecule per cavity at low loadings (average bulk loading ≤1 molecule per cavity) and two molecules per cavity at higher loadings.

Introduction

Because of their high internal surface areas and molecular size cage dimensions, zeolites are used widely as shape-selective catalysts or adsorbents in a variety of industrially significant chemical processes.[1,2] Transport and adsorption of reactant species within the porous zeolite matrix are particularly crucial to the molecular sieve function of these materials. Heterogeneous catalytic processes, for example, rely on molecular clustering and orientation at surface adsorption sites to promote chemical reactions. The diffusivity and adsorption kinetics of reactant guest molecules in zeolites are known, however, to be highly dependent on treatment conditions that have a dramatic effect on the distribution of guest molecules within the porous matrix. In probing the kinetics of such phenomena at the molecular level, it is imperative that the distribution and dynamic behavior of adsorbed species be understood in porous materials.

Hydrocarbons adsorbed on zeolites have been extensively studied by X-ray scattering,[3] infrared spectroscopy,[4] and neutron diffraction[5] which, if taken together, provide insight into the distribution, mobility, and orientation of organic guest species. Applications of NMR techniques to the study of zeolites are widespread and are reviewed in numerous texts.[6] Although the molecular dynamics of simple molecules, such as water, methane, benzene, and xenon, adsorbed in zeolite cavities have been investigated by using NMR relaxation times,[7] line-shape analyses,[8] and pulsed field-gradient experiments,[9,10] local structural information pertinent to adsorbate distribution is not easily obtained. Important questions remain with regard to the uniformity, site occupancy, and preparatory treatment dependence of adsorbate distributions in zeolite cavities.

To address these issues, we have employed a combination of ^{129}Xe and proton multiple-quantum NMR to obtain detailed information on the distributions of adsorbed organic molecules in NaY zeolite. By virtue of a ^{129}Xe chemical shift range that exceeds 5000 ppm, slight variations in local environment can have a profound influence on the ^{129}Xe resonance frequency. Fraissard and co-workers,[11,12] Ripmeester,[13] Pines et al.,[14] and others[15] have successfully applied ^{129}Xe NMR to the study of ordered porous materials, such as zeolites and clathrates, with and without guest species. Multiple-quantum (MQ) NMR spectroscopy[16] provides a convenient way of determining the size of hydrogen clusters[17] within isolated NaY supercages from which organic guest occupancies of the zeolite cavities can be inferred.

In a preliminary communication,[18] we described the application of ^{129}Xe and multiple-quantum NMR techniques to the study of

† Present address: Institute of Atomic and Molecular Sciences, Academia Sinica, P.O. Box 23-166, Taipei, Taiwan, R.O.C.

‡ Present address: Department of Chemistry, Korea Advanced Institute of Science and Technology, Taejon 305-71, Korea.

§ Present address: Laboratoire de Chimie Organique Physique et Cinetique Chimique Appliquées, UA 418 C.N.R.S., ENSCM, 3 rue Ecole Normale, 34075 Montpellier Cedex, France.

(1) Breck, D. W. *Zeolite Molecular Sieves*; Krieger: Malabar, FL, 1984.
(2) Barrer, R. M. *Zeolites and Clay Minerals as Sorbents and Molecular Sieves*; Academic Press: New York, 1978.
(3) Amaro, A. A.; Seff, K. *J. Phys. Chem.* **1973**, *77*, 906.
(4) (a) Cohen de Lara, E. In *Proceedings of the Fifth International Conference on Zeolites*; Rees, L. V. C., Ed.; Heyden: London, 1980; p 414. (b) O'Malley, P. J. *Chem. Phys. Lett.* **1990**, *166*, 340.
(5) See for example: (a) Kahn, R.; Cohen de Lara, E.; Thorel, P.; Ginoux, J. L. *Zeolites* **1982**, *2*, 260. (b) Stockmeyer, R. *Zeolites* **1984**, *4*, 81. (c) Wright, P. A.; Thomas, J. M.; Ramdas, S.; Cheetham, A. K. *J. Chem. Soc., Chem. Commun.* **1984**, *5*, 1338. (d) Fitch, A. N.; Jobic, H.; Renouprez, A. *J. Phys. Chem.* **1986**, *90*, 1311. (e) Taylor, J. C. *Zeolites* **1987**, *7*, 311.
(6) (a) Fyfe, C. A. *Solid State NMR for Chemists*; CFC Press: Guelph, Ontario, Canada, 1983. (b) Klinowski, J. *Prog. Nucl. Magn. Reson. Spectrosc.* **1984**, *16*, 237. (c) Thomas, J. M.; Klinowski, J. *Adv. Catal.* **1985**, *33*, 199. (d) Engelhardt, G.; Michel, D. *High-Resolution Solid State NMR of Silicates and Zeolites*; Wiley: New York, 1987.
(7) (a) Resing, H. A. *Adv. Mol. Relax. Processes* **1972**, *3*, 199. (b) Geschke, D.; Pfeifer, H. *Z. Phys. Chem. (Leipzig)* **1976**, *257*, 365. (c) Basler, W. D.; Lechert, H.; Weyda, H. *Catal. Today* **1988**, *3*, 31.
(8) (a) Hoffmann, W. D. *Z. Phys. Chem. (Leipzig)* **1976**, *257*, 315. (b) Lechert, H.; Wittern, K. P. *Ber. Bunsen-Ges. Phys. Chem.* **1978**, *82*, 1054. (c) Eckman, R.; Vega, A. J. *J. Am. Chem. Soc.* **1983**, *105*, 4841. (d) Boddenberg, B.; Burmeister, R. *Zeolites* **1988**, *8*, 488. (e) Burmeister, R.; Boddenberg, B.; Verfürden, M. *Zeolites* **1989**, *9*, 318. (f) Silbernagel, B. G.; Garcia, A. R.; Newsam, J. M.; Hulme, R. *J. Phys. Chem.* **1989**, *93*, 6506.
(9) Kärger, J.; Pfeifer, H.; Heink, W. *Advances in Magnetic Resonance*; Waugh, J., Ed.; Academic Press: San Diego, 1988; p 1.
(10) Heink, W.; Kärger, J.; Pfeifer, H.; Stallmach, F. *J. Am. Chem. Soc.* **1990**, *112*, 2175.
(11) For ^{129}Xe NMR studies of xenon adsorbed in zeolites: (a) Ito, T.; Fraissard, J. *J. Chem. Phys.* **1982**, *76*, 5225. (b) Ito, T.; de Menorval, L. C.; Guerrier, E.; Fraissard, J. P. *Chem. Phys. Lett.* **1984**, *111*, 271. (c) Springuel-Huet, M. A.; Ito, T.; Fraissard, J. P. *Structure and Reactivity of Modified Zeolites*; Studies in Surface Science and Catalysis Series 18; Jacobs, P. A.; et al., Eds.; Elsevier: Amsterdam, 1984; p 13.
(12) For ^{129}Xe NMR studies of xenon adsorbed in metal-loaded zeolites: (a) de Menorval, L. C.; Fraissard, J. P.; Ito, T. *J. Chem. Soc., Faraday Trans. 1* **1982**, *78*, 403. (b) Fraissard, J.; Ito, T.; de Menorval, L. C. In *Proceedings of the Eighth International Congress on Catalysis*; Verlag-Chemie: Weinheim, 1985; Vol. 3, p 25. (c) de Menorval, L. C.; Fraissard, J.; Ito, T.; Primet, M. *J. Chem. Soc., Faraday Trans. 1* **1985**, *81*, 2855.
(13) (a) Ripmeester, J. A.; Davidson, D. W. *J. Mol. Struct.* **1981**, *75*, 67. (b) Ripmeester, J. A. *J. Am. Chem. Soc.* **1982**, *104*, 289. (c) Ripmeester, J. A. *J. Magn. Reson.* **1984**, *56*, 247.
(14) (a) Chmelka, B. F.; Ryoo, R.; Liu, S. B.; de Menorval, L. C.; Radke, C. J.; Petersen, E. E.; Pines, A. *J. Am. Chem. Soc.* **1988**, *110*, 4465. (b) de Menorval, L. C.; Raftery, D.; Liu, S. B.; Takegoshi, K.; Ryoo, R.; Pines, A. *J. Phys. Chem.* **1990**, *94*, 27.
(15) (a) Scharpf, E. W.; Crecely, R. W.; Gates, B. C.; Dybowski, C. *J. Phys. Chem.* **1986**, *90*, 9. (b) Shoemaker, R.; Apple, T. *J. Phys. Chem.* **1987**, *91*, 4024. (c) Davis, M. E.; Saldarriaga, C.; Montes, C.; Hanson, B. E. *J. Am. Chem.* **1988**, *92*, 2557. (d) Samant, M. G.; de Menorval, L. C.; Dalla-Betta, R. A.; Boudart, M. *J. Phys. Chem.* **1988**, *92*, 3937. (e) Derouane, E. G.; Davis, M. E. *J. Mol. Catal.* **1988**, *48*, 37.
(16) (a) Pines, A. In *Proceedings of the 100th School of Physics "Enrico Fermi"*; Maraviglia, B., Ed.; North-Holland: Amsterdam, 1988; p 43. (b) Munowitz, M.; Pines, A. *Science* **1986**, *233*, 525.

0022-3654/91/2095-0303$02.50/0

NaY zeolite samples containing adsorbed hexamethylbenzene (HMB). These experiments demonstrated the importance of sample heat treatment in the distribution of organic guest species within NaY zeolite cavities. Such information is crucial to understanding the reaction performance of zeolite catalysts used in transalkylation processes, for example, the production of xylene from alkylbenzene species.[19] Here, we present a complete account of this work and extend the study to distributions of adsorbed benzene and 1,3,5-trimethylbenzene (TMB) in NaY zeolite. These particular molecules were chosen because their kinetic diameters, 0.58 nm for benzene, 0.75 nm for TMB, and 0.82 nm for HMB, are comparable to the 0.74-nm supercage aperture of NaY at room temperature.[1] The relevance of molecular size, mobility, and phase properties to the transport and adsorption of organic guests can therefore be investigated. The combination of ^{129}Xe and multiple-quantum NMR comprehensively characterizes the distributions of these adsorbate species, not only among a collection of sample particles but also within individual NaY zeolite particles as well.

Experimental Section

All zeolite samples were prepared in 10-mm NMR tubes connected to a vacuum apparatus through a high-vacuum stopcock. NaY zeolite was synthesized according to the procedure of Breck,[1] with crystallinity confirmed by X-ray diffraction studies. Separate scanning electron microscope experiments established NaY crystallite grain diameters of 1–2 μm.[20] Before addition of the adsorbate species, the NaY samples were dehydrated in the sample tubes by heating at 673 K under vacuum (ca. 10^{-5} Torr) overnight. After dehydration, a known amount of organic adsorbate was introduced to the zeolite at room temperature to achieve the bulk loading desired. Adsorbate loadings were calculated from mass balances utilizing NaY supercage density and the masses of zeolite and organic guest materials. Benzene was introduced to NaY zeolite samples at room temperature by allowing benzene vapor to diffuse into the bed under evacuated conditions. Liquid TMB and solid HMB were stored at 273 K in a side arm of the sample tube during dehydration and subsequently introduced mechanically under vacuum to the top of the zeolite sample volume. Without delay, the samples were placed in a furnace equipped with a programmable temperature controller, heated for a known period of time, and cooled to room temperature over a period of many hours. Xenon gas was then introduced into each sample at room temperature and allowed to equilibrate to a pressure of $\approx$300 Torr.

Room-temperature ^{129}Xe NMR spectra were obtained on spectrometers operating at 49.8 and 110.0 MHz. Each acquisition typically consisted of 2000–4000 free induction decay scans with a delay of 0.5 s between 90° pulses. The experiments employed a sweep width of 41 667 Hz with a digitizing time of 12 μs. All ^{129}Xe chemical shift values are referenced to the ^{129}Xe signal of xenon gas at very low pressure[21] and are believed accurate to 0.5 ppm. Proton multiple-quantum NMR data were obtained by using a phase cycling technique[17] on a home-built spectrometer operating at 179 MHz. Long excitation time multiple-quantum intensities were fit to a Gaussian curve according to statistical arguments described elsewhere.[22] The effective cluster size N is obtained from the standard deviation of the Gaussian fit, taken equal to $(N/2)^{1/2}$.

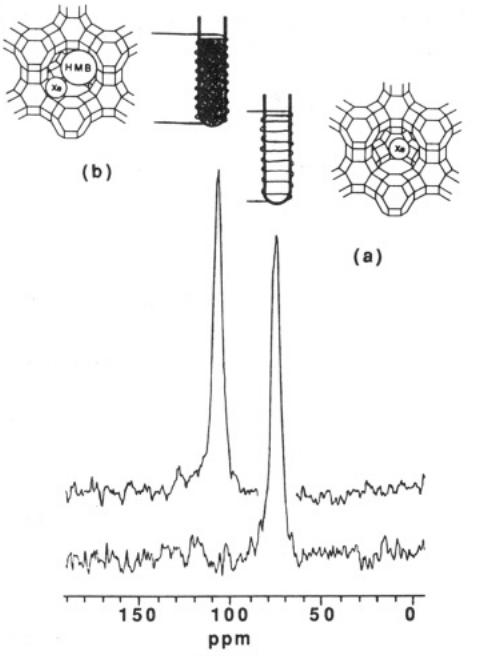

Figure 1. Room-temperature ^{129}Xe NMR spectra of xenon (300-Torr equilibrium pressure) adsorbed on dehydrated NaY zeolite with and without adsorbed HMB guest species. Schematic diagrams of NaY zeolite samples in 10-mm NMR tubes are shown above the spectra. Shading reflects the presence of adsorbed guests in supercage environments. The molecular guests occupying the supercages are not shown to scale. The receiver coil is shown to indicate the approximate sample volume probed by the NMR experiment. (a) The ^{129}Xe chemical shift, δ_{Xe}, is 78 ppm in dehydrated NaY containing no guest species. (b) δ_{Xe} = 109 ppm in dehydrated NaY containing, on average, one HMB molecule per supercage adsorbed at 523 K.

Macroscopic Adsorbate Distributions

As a sensitive, nonreactive probe of supercage cavities within the crystalline zeolite matrix, room-temperature ^{129}Xe NMR provides information on interparticle adsorbate distribution heterogeneities in polycrystalline NaY samples. Physisorption within the zeolite matrix perturbs a xenon atom's spherical, polarizable electron cloud, producing a shift in the ^{129}Xe resonant frequency in an externally applied magnetic field. In NaY zeolite, the 0.44-nm xenon atoms easily penetrate the 0.74-nm windows into the supercages, thereby serving as an indirect probe of guest molecules adsorbed in supercage sites. The room-temperature ^{129}Xe NMR spectrum of xenon adsorbed on dehydrated NaY zeolite is shown in Figure 1a. The single line at 78 ppm agrees with that found previously by Ito and Fraissard for xenon adsorbed on NaY at an equilibrium xenon pressure of 300 Torr.[23] The large downfield shift in the ^{129}Xe resonance is a result of the deshielding experienced by ^{129}Xe nuclei due to collisions of xenon atoms with the NaY cage walls and with other xenon atoms. Figure 1b displays a ^{129}Xe NMR spectrum containing a single peak at 109 ppm corresponding to xenon adsorbed on dehydrated NaY zeolite loaded with an average of 1.0 HMB molecule per supercage. As demonstrated in our preliminary communication[18] and recently by Gedeon et al.,[24] sample heat treatment plays a crucial role in controlling the distribution of the adsorbed guest molecules within the zeolite sample.

HMB in NaY

It is possible, using ^{129}Xe NMR, to distinguish between a packed bed of zeolite crystallites possessing an axial adsorbate concentration gradient and one in which the adsorbate is dispersed homogeneously throughout the macroscopic sample volume. This is accomplished by exploiting the different perturbations experienced by xenon atoms diffusing through zeolite environments containing different guest loadings. By monitoring the chemical

(17) (a) Baum, J.; Pines, A. *J. Am. Chem. Soc.* **1986**, *108*, 7447. (b) Munowitz, M.; Pines, A.; Mehring, M. *J. Chem. Phys.* **1987**, *86*, 3172. (c) Shykind, D. N.; Baum, J.; Liu, S. B.; Pines, A.; Garroway, A. N. *J. Magn. Reson.* **1988**, *76*, 149.

(18) Ryoo, R.; Liu, S. B.; de Menorval, L. C.; Takegoshi, K.; Chmelka, B.; Trecoske, M.; Pines, A. *J. Phys. Chem.* **1987**, *91*, 6575.

(19) (a) Kaeding, W. W.; Chu, C.; Young, L. B.; Butter, S. A. *J. Catal.* **1981**, *69*, 392. (b) Wei, J. *J. Catal.* **1982**, *76*, 433. (c) Kuei-jung, C.; Leu, L. *Zeolites* **1989**, *9*, 193.

(20) Chmelka, B. F. Ph.D. Dissertation, University of California, Berkeley, CA, May 1990.

(21) Fraissard, J.; Ito, T.; de Menorval, L. C.; Spinguel-Huet, M. A. In *Metal Microstructures in Zeolites: Preparation, Properties, Applications*; Studies in Surface Science and Catalysis Series 12; Jacobs, P.A., et al., Eds.; Elsevier: Amsterdam, 1982; p 179.

(22) Munowitz, M. *Coherence and NMR*; Wiley: New York, 1988.

(23) Ito, T.; Fraissard, J. *J. Chem. Phys.* **1982**, *76*, 5225.

(24) Gedeon, A.; Ito, T.; Fraissard, J. *Zeolites* **1988**, *8*, 376.

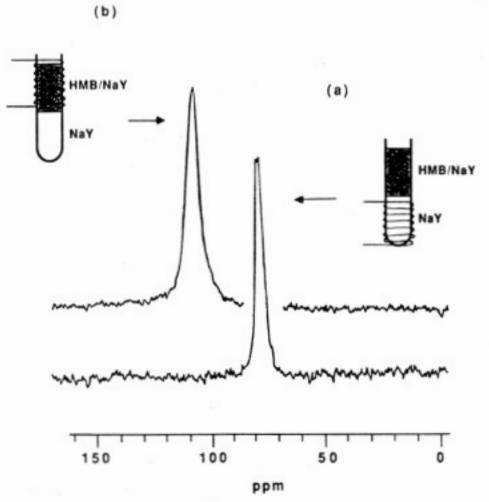

Figure 2. Room-temperature ^{129}Xe NMR spectra of xenon (300-Torr equilibrium pressure) adsorbed on dehydrated NaY zeolite containing a bulk loading of 0.5 HMB molecule per supercage. The HMB was adsorbed onto the zeolite by heating at 523 K for 2 h. (The adsorbate distribution remains unaffected by longer heating periods.) Different zones of the zeolite bed can be probed by varying the position of the receiver coil relative to sample: (a) δ_{Xe} = 78 ppm near the bottom of the sample, while (b) δ_{Xe} = 109 ppm in the uppermost region.

shift of physisorbed ^{129}Xe, one can identify distinct zones of guest molecule adsorption within NaY zeolite samples. Figure 2, for example, displays ^{129}Xe spectra of xenon adsorbed at 295 K on dehydrated NaY containing, on average, one molecule of HMB for every two supercage cavities present in the bulk sample (denoted hereafter as 0.5 HMB/cavity). Placement of the receiver coil about the lower region of the sample volume results in the single ^{129}Xe peak at 78 ppm shown in Figure 2a. From comparison with Figure 1a, this corresponds to xenon adsorbed in NaY supercage cavities devoid of HMB guests. Conversely, placement of the receiver coil about the uppermost region of the sample volume results in a single ^{129}Xe peak at 109 ppm (Figure 2b) corresponding to xenon adsorbed in supercages containing HMB guests. The identical ^{129}Xe chemical shift values observed in Figures 1b and 2b indicate the existence of a single HMB molecule per supercage in the upper region of the NaY zeolite bed.

This methodology can be extended to sample volumes containing different adsorbate loadings and/or different adsorbate guest species. Figure 3 depicts ^{129}Xe NMR spectra for different loadings of HMB introduced into the NaY matrix at 523 K and then redistributed at 573 K. In Figure 3a, the two peaks at 109 and 78 ppm correspond to distinct adsorption zones with and without HMB guest species adsorbed in NaY supercage cavities. The chemical shifts of these peaks are identical with those in Figure 1 for NaY samples loaded with one and zero HMB molecules per NaY supercage, respectively. It is clear, therefore, that zeolite particles in the upper region of the sample volume contain one HMB molecule per supercage, whereas those in the lower region are devoid of adsorbed guests. The well-resolved peaks indicate close to a step change in HMB concentration near the midpoint of the sample volume's longitudinal axis. The nearly equal peak areas reflect a nearly equal number of xenon adsorption sites in the two regions, as expected for an average bulk loading of 0.5 HMB/cavity. Upon reheating this sample to 573 K for 4 h, the discrete lines in Figure 3a collapse to the single peak in Figure 3d at 94 ppm. This is consistent with dispersal of HMB throughout the sample volume and indicates a macroscopically uniform guest distribution. In this situation, xenon atoms diffusing rapidly from one supercage to another encounter equal numbers of empty and HMB-occupied cavities; hence, the 94-ppm chemical shift is the expected arithmetic average of ^{129}Xe shift values in the presence of only empty NaY cavities (78 ppm) or only cavities with one HMB guest (109 ppm).

Similar results are obtained for samples containing higher adsorbed guest loadings, as shown in Figure 3b,c,e,f. As the overall

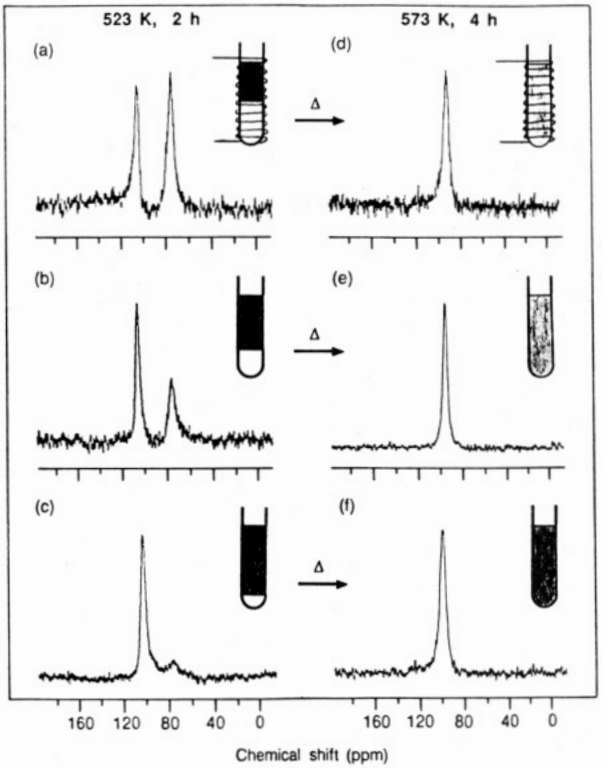

Figure 3. Xenon-129 NMR spectra of xenon (300-Torr equilibrium pressure) adsorbed on dehydrated NaY zeolite containing (a) 0.5, (b) 0.7, and (c) 0.9 HMB molecule per supercage. The samples in (a)–(c) were all initially heated at 523 K for 2 h. Spectra d–f were obtained after reheating the respective samples at 573 K for 4 h. Macroscopic adsorbate distributions in the samples are reflected in the schematic diagram accompanying each spectrum.

TABLE I: Some Properties of Benzene and Related Compounds

	kinetic diameter, nm	normal melting point, K	normal boiling point, K
benzene	0.58	279	353
1,3,5-trimethylbenzene	0.75	318	438
hexamethylbenzene	0.82	440	538

adsorbate loading increases, the intensity of the line arising from xenon adsorbed in the presence of one HMB guest at 109 ppm increases relative to that from xenon adsorbed in empty NaY supercages at 78 ppm (Figure 3a–c). After a 2-h heat treatment at 523 K, a bulk loading of 0.7 HMB/NaY supercage yields ^{129}Xe peaks at 109 and 78 ppm (Figure 3b) with relative areas of approximately 0.7 and 0.3, respectively. These data are consistent with 1 HMB/supercage in the upper 70% of the zeolite sample volume, with the remainder being devoid of adsorbed molecular species. Further heating of this sample for 4 h at 573 K disperses the organic guests throughout the macroscopic sample volume, yielding the single ^{129}Xe peak at 98 ppm in Figure 3e. The peak location is again very close to the average of the ^{129}Xe resonance signals with and without HMB present, weighted by the respective bed fractions of the two zones.

Similarly, a bulk loading of 0.9 HMB/NaY supercage after thermal treatment at 523 K yields the ^{129}Xe spectrum shown in Figure 3c with peaks at 109 and 78 ppm. Again, the relative areas of the two peaks, approximately 0.9 and 0.1, reflect the proportions of the macroscopic sample volume with and without an HMB guest adsorbed in the NaY supercages. After thermal treatment at 573 K, the two peaks collapse in Figure 3f as before to a single peak at 102 ppm near the expected weighted-average location.

TMB and Benzene in NaY

Introduction of chemically similar 1,3,5-trimethylbenzene (TMB) and benzene into the NaY supercage network yields results

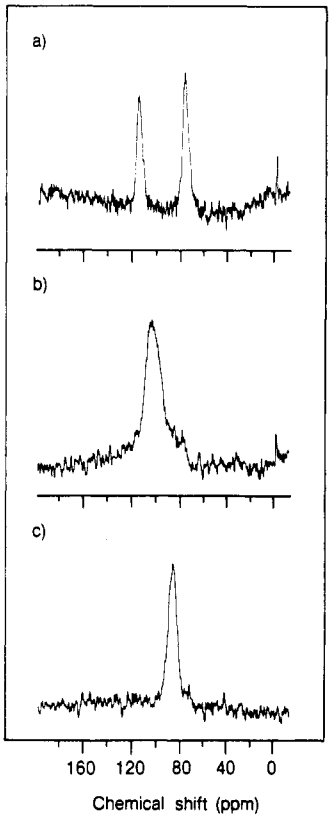

Figure 4. Xenon-129 NMR spectra of xenon (300-Torr equilibrium pressure) adsorbed on dehydrated NaY zeolite containing 0.5 molecule of 1,3,5-trimethylbenzene (TMB) per supercage: (a) sample heated at 323 K for 0.5 h; (b) same sample heated again at 413 K for 1 h; (c) after further heating at 523 K for 2 h. The xenon gas peak at ≈0 ppm is seen in both (a) and (b).

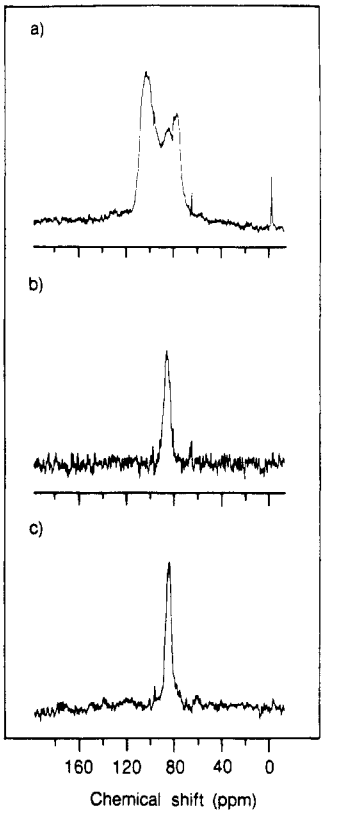

Figure 5. Xenon-129 NMR spectra of xenon (300-Torr equilibrium pressure) adsorbed on dehydrated NaY zeolite containing 0.5 benzene molecule per supercage. (a) Benzene adsorbed at 298 K. The narrow peak at ≈0 ppm arises from gaseous xenon in the interstitial voids between zeolite particles. (b) The same sample heated at 423 K for 1 h and (c) after further heating at 473 K for 1 h.

that are consistent with the above discussion. Table I demonstrates that the melting and boiling points of bulk TMB and benzene are significantly lower than those of HMB. Accordingly, less severe thermal treatments are necessary to effect transport and subsequent adsorption of the guest species within the sample volume.[25] Elevated guest concentrations in the macropores between zeolite particles induce dispersal of the guest species through the bed at temperatures lower than those studied for HMB.

Figure 4 displays ^{129}Xe NMR spectra of NaY zeolite samples containing a bulk average of approximately 0.5 TMB molecule/supercage adsorbed under progressively more severe thermal conditions. After initial heat treatment at 323 K for 0.5 h, two distinct lines of roughly equal intensity are observed at 116 and 78 ppm in the ^{129}Xe spectrum of Figure 4a. Again, the peak at 78 ppm is attributed to the ^{129}Xe chemical shift in empty NaY supercages, while that at 116 ppm is from ^{129}Xe in cavities containing one TMB guest. A loading of 0.5 TMB molecules per cavity produces peaks of roughly equal intensity because one-half of the NaY supercages are empty and the other half contain one molecule of TMB. This corresponds to an axial TMB concentration gradient in the zeolite bed analogous to that for the HMB/NaY system shown in Figure 3a.

Further heating of this sample for 1 h at 413 K yields a broad ^{129}Xe peak at 105 ppm with a noticeable shoulder at about 78 ppm (Figure 4b). The broadness of the spectrum reflects an intermediate adsorbate distribution somewhere between the sharp macroscopic heterogeneity of Figure 4a and the homogeneous guest dispersion of Figure 4c. At 413 K, desorption of TMB from supercage sites in the upper portion of the zeolite bed allows the guest species to diffuse into the lower reaches of the sample volume. After additional heat treatment at 523 K for 2 h, Figure 4c reveals a single sharp line at 88 ppm which indicates complete dispersal of TMB throughout the macroscopic sample volume. These observations are consistent with the ^{129}Xe NMR data in Figure 3 for the HMB/NaY system.

From the arguments presented above, we expect a similar thermal treatment dependence for benzene introduced into polycrystalline NaY zeolite. Figure 5a depicts the ^{129}Xe NMR spectrum for a NaY sample containing 0.5 benzene molecule per supercage chemisorbed at room temperature. A high concentration of benzene in the macropores between NaY crystallites results in substantial benzene transport to the lower reaches of the bed, even at room temperature.[25] The nonzero signal intensity between peaks observed at 106 and 78 ppm indicates that the macroscopic sample heterogeneity is not a sharp front as before. Instead, the data reflect an ensemble of particles that contain a gradually decreasing number of benzene molecules across a diffuse boundary between adsorption zones with and without organic guest species. The peak at 78 ppm is assigned unambiguously to xenon atoms in the empty NaY zeolite cavities, as in Figure 1a. The remaining two peaks at 86 and 106 ppm arise from xenon atoms in NaY cavities containing one or more benzene molecules, respectively. After heating the sample at 423 K for 1 h the multiple peaks of Figure 5a collapse to a single resonance at 89 ppm (Figure 5b). Further heating at 473 K for 1 h results in a slightly narrower line at 87 ppm (Figure 5c). Apart from the small difference in ^{129}Xe peak locations in Figure 5b,c, the chemical shifts are near the weighted-average value expected from the spectrum in Figure 5a. Above 473 K, dispersal of benzene guests throughout the sample volume is consistent with thermal desorption experiments which document benzene desorption from faujasite-type zeolites above 460 K.[26] Subsequent sample heating at 533 K for 2 h yields a spectrum identical with Figure 5c. Samples containing 1.5 benzene molecules per cavity behaved similarly.

(25) Chmelka, B. F.; Gillis, J. V.; Petersen, E. E.; Radke, C. J. *AIChE J.* **1990**, *36*, 1562.

(26) (a) Fominykh, L. F.; Shaburo, I. S.; Artem'eva, A. F. *Neftepererab. Neftekhim. (Moscow)* **1974**, *7*, 39. (b) Choudhary, V. R.; Srinivasan, K. R.; Akolekar, D. B. *Zeolites* **1989**, *9*, 115.

Heterogeneity Length Scales by ^{129}Xe NMR

Because the length scale of the zeolite guest heterogeneity is important to the utility of the ^{129}Xe NMR technique, establishing the mobility of xenon probe atoms during the experiment is crucial to the distribution heterogeneity measurement. For samples that possess fewer than one guest molecule per supercage, some cavities contain guest molecules while others do not. One might, therefore, expect to observe two or more ^{129}Xe NMR signals corresponding to cavities with or without adsorbed guest species. At 298 K and 300 Torr, the mean free path of gaseous xenon is calculated from kinetic theory to be approximately 142 nm. Within the 1.25-nm-diameter NaY supercages, therefore, the use of bulk transport properties ($D \approx 10^{-5}$ m^2/s) (ref 27) overestimates the mobility of the xenon probe species.

The macroscopic guest distribution heterogeneities in Figure 3a–c produce two well-resolved peaks reflecting slow exchange of xenon between the two adsorption environments. The relevant time scale in these experiments is the reciprocal frequency separation of the ^{129}Xe peaks corresponding to xenon adsorption sites in NaY supercages with and without HMB.[28] In Figure 3a, for example, ^{129}Xe resonances in the two environments are separated by 31 ppm (3400 Hz), for which an exchange time of 290 μs results. We define the length scale of a particular distribution heterogeneity to be the mean distance between supercages with and without an adsorbed guest. In Figures 2 and 3a–c, the distances separating supercages with and without HMB are large, so that jumps between these environments occur on a time scale that is slow with respect to 290 μs.[29] On the other hand, microscopic guest distribution heterogeneities resulting from heat treatment of HMB/NaY samples at 573 K produce a single peak, as shown in Figure 3d–f. Rapid xenon exchange between adjacent supercages with and without HMB averages the contributions from the two environments. Jumps between the different sites occur significantly faster than 290 μs, since little broadening is observed.

The issue, then, centers on the magnitude of the heterogeneity length scales that can be probed in NaY zeolite by the ^{129}Xe NMR technique. To address the issue of xenon mobility in NaY, we consider two limiting cases corresponding to diffusion of a xenon probe atom within a single crystallite or among several crystallites during the NMR experiment. Figure 6 depicts anticipated ^{129}Xe NMR spectra for these two possibilities: first, in the presence of an axial HMB concentration gradient and, second, after thorough mixing of the particles to render the sample volume homogeneous in macroscopic terms. At room temperature the adsorbed HMB molecules are strongly bound, so that the adsorbed guest population of each crystallite is the same prior to and after physical mixing; only the relative particle positions within the bed are changed. Suppose that xenon atoms diffuse too slowly to probe more than an average supercage environment within a single micron-size zeolite particle. Such xenon atoms occupy only one crystallite on the time scale of the NMR experiment and, therefore, must be indifferent to the adsorbed guest loadings in adjacent particles. Consequently, as shown in Figure 6a, physical mixing of a zeolite sample containing a macroscopically heterogeneous adsorbate distribution should not alter the ^{129}Xe NMR spectrum in any way.

Conversely, if xenon atoms diffuse rapidly enough to visit many particles on the time scale of the NMR experiment, a more macroscopic averaging of the resonance signal is expected. As illustrated in Figure 6b, the ^{129}Xe NMR technique would be then capable of resolving adsorbate distribution heterogeneities with length scales no smaller than several crystallite diameters. The xenon atoms in such circumstances would be sensitive to the adsorbed guest loadings of adjacent crystallites whose placement

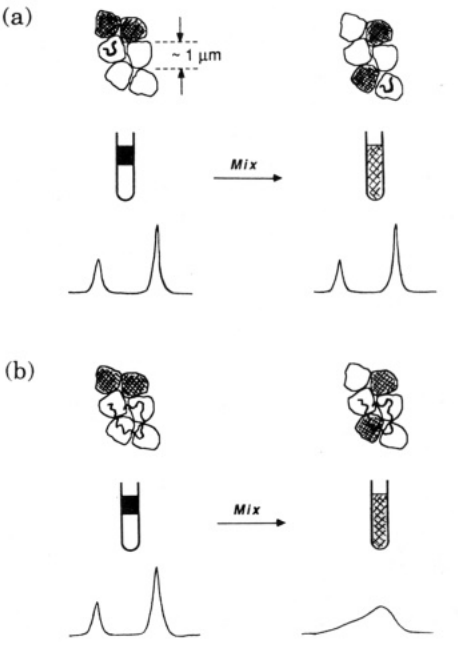

Figure 6. Schematic diagrams of ^{129}Xe NMR spectra expected for different xenon mobilities in NaY zeolite containing 0.3 guest molecule per supercage. A xenon atom diffuses (a) within a single crystallite or (b) among several adjacent crystallites on the time scale of the NMR experiment. Shading indicates that the particles are occupied by adsorbed guest species, with the macrocopic distribution of such particles (in 10-mm NMR tubes) also shown, before and after mechanical mixing.

in the bed is disturbed by the mixing process. As a consequence of physically mixing the bed, the ^{129}Xe NMR spectrum would thus collapse to the single peak shown in Figure 6b. Rapid xenon exchange among many particles containing different HMB loadings would average the ^{129}Xe resonance from an ensemble of particles in close proximity to one another. This situation is similar to a thermally mixed HMB/NaY system in that the respective distribution heterogeneities are unresolved as a result of high xenon mobility within the samples (Figure 3d–f).

Xenon mobility in HMB/NaY can be established experimentally by the sample-mixing procedure discussed above. Because the macroscopic HMB distribution heterogeneities arising from chemisorption of HMB in NaY at 523 K are large (Figure 3a–c), exchange is slow between adsorption zones with and without HMB. Physically mixing the zeolite particles in such a sample alters the bed character by reducing the heterogeneity length scale to that of several crystallite diameters; the mechanical mixing procedure is not 100% efficient, yielding a collection of aggregates comprised of a smaller number of zeolite particles. Xenon-129 NMR data shown in Figure 7, for NaY zeolite containing 0.3 HMB/supercage adsorbed at 523 K, reveal that thorough mixing of the NaY particles within the sample produces little change in the ^{129}Xe spectrum from that obtained in the presence of a macroscopic axial distribution of HMB. This clearly indicates that xenon exchange between aggregates is slow compared to the 290-μs exchange time between adsorption environments. Since Figure 3d–f reflect rapid xenon exchange among many adjacent supercages, we have bounded xenon mobility to occur within several crystallites on the time scale of the NMR experiment. When either multiple or broad ^{129}Xe lines are observed, the length scales of the sample's heterogeneities must be, consequently, larger than several NaY crystallite diameters ($\approx$10 μm). The ^{129}Xe peaks in these regions are resolved or broadened due to slow exchange between the adsorption zones reflecting, thereby, the macroscopic nature of the heterogeneous guest distribution. It is clear that room-temperature ^{129}Xe NMR is, thus, capable of resolving heterogeneous distributions of molecular species in NaY zeolite, providing the length scales of the heterogeneities are larger than approximately 10 μm.

With the characteristic length, l, and time, t, of the xenon exchange process known in NaY, a diffusivity calculation permits

(27) Reid, R. C.; Prausnitz, J. M.; Sherwood, T. K. *The Properties of Gases and Liquids*; McGraw-Hill: New York, 1977.

(28) (a) Kaplan, J. I.; Fraenkel, G. *NMR of Chemically Exchanging Systems*; Academic Press: New York, 1980. (b) Freeman, R. *A Handbook of Nuclear Magnetic Resonance*; Wiley: New York, 1987.

(29) (a) Abragam, A. *Principles of Nuclear Magnetism*; Clarendon Press: Oxford, 1961. (b) Carrington, A.; McLachlan, A. D. *Introduction to Magnetic Resonance*; Harper and Row: New York, 1967.

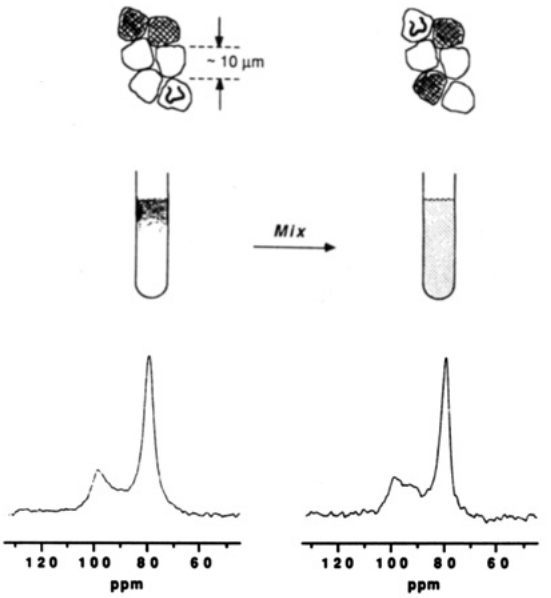

Figure 7. Room-temperature ^{129}Xe NMR spectra of xenon (300-Torr equilibrium pressure) adsorbed on partially hydrated NaY zeolite containing a bulk loading of 0.3 HMB molecule per supercage adsorbed at 523 K for 2 h. Spectra were acquired before and after thorough physical mixing of the sample. In the schematic diagrams, each aggregate represents a collection of a small number of crystallites that remain grouped together during the mechanical mixing process. Shading again indicates that the particles are occupied by adsorbed guest species.

the mobility of the sorbed ^{129}Xe probe to be made more quantitative. Using Einstein's equation[30]

$$\langle l(t)^2 \rangle = 6D_{Xe}t$$

with $t = 290$ μs and $l(t) = 10$ μm, we estimate the self-diffusivity of xenon in NaY zeolite, D_{Xe}, to be 6×10^{-8} m^2/s at 298 K. This value is consistent with recent NMR pulsed field-gradient measurements of xenon mobility in NaX[10] and with molecular dynamics simulations of xenon in silicalite.[31] At reduced temperatures, we note that diminished mobility of xenon atoms may permit zeolite heterogeneities on the order of 1 μm to be probed using ^{129}Xe NMR.[32]

For heterogeneities characterized by length scales significantly smaller than 1–10 μm, detailed information on intracrystalline guest distributions is, unfortunately, not readily obtained by room-temperature ^{129}Xe NMR spectroscopy. The single peaks present in the ^{129}Xe spectra of Figure 3d–f, for instance, are consistent with both of the intracrystalline distributions shown in Figure 8. The length scales of the adsorbate distribution heterogeneities in the two cases are both very small compared to individual NaY crystallite diameters. At room temperature, fast hopping of the xenon atoms among the cavities with and without guest molecules averages the ^{129}Xe chemical shift values of the various adsorption environments. To examine smaller adsorbate distribution length scales, we use multiple-quantum NMR to assess proton cluster sizes in the NaY cavities.

Intracrystalline Adsorbate Distributions

As discussed above, dispersal of adsorbed HMB guests throughout the sample volume results in much smaller heterogeneity length scales than can be distinguished by the highly mobile ^{129}Xe probe species at room temperature. Adsorption of 0.5 HMB molecules per NaY supercage at 573 K, for instance, results in a nominal heterogeneity length scale on the order of 1 nm, the distance between adjacent supercages in the NaY matrix. Also, at this temperature, the kinetic barrier to chemisorption of at least a second HMB molecule in each supercage is surmounted, so that clustering of guest species may occur.[18] By establishing the number of adsorbed organic molecules residing in NaY supercages, multiple-quantum NMR probes guest distribution heterogeneities on a molecular scale.

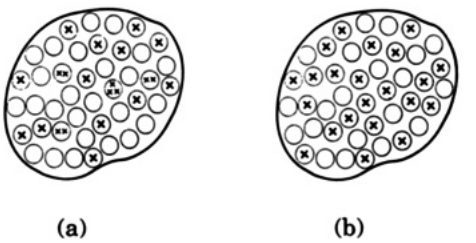

Figure 8. Schematic diagrams of possible guest molecule distributions within the cavities of a single zeolite crystallite when the average loading is less than one molecule per cavity. The open circles represent empty zeolite cavities, and the guest molecules are indicated by the symbol ×. (a) Statistical distribution of adsorbed guest molecules in zeolite supercage cavities. (b) Homogeneous dispersion in which each zeolite supercage contains at most one adsorbed guest molecule.

Multiple-Quantum NMR Studies of Spin Clustering

The multiple-quantum "counting" experiment is sensitive to the average size of homonuclear dipole–dipole coupled spin networks in a given sample.[16,17] The two intracrystalline guest distributions of Figure 8 are distinguished by the manner in which the adsorbed guest species are distributed in NaY supercages. In Figure 8a, the adsorbate is statistically dispersed, with some cavities containing two or perhaps three molecules, though the bulk average remains 0.5 guest/supercage. This is in contrast to the homogeneous guest dispersion shown in Figure 8b, where only one adsorbed molecule is present in each occupied supercage at an identical 0.5 guest/supercage bulk loading. Each guest molecule possesses a collection of dipole–dipole coupled protons that couple to the protons on other nearby molecules. Such intermolecular proton coupling, however, will be much stronger between guest species occupying the same supercage than between molecules in separate cavities. The collection of guests adsorbed in each supercage can, therefore, be modeled as an isolated network of N dipole–dipole coupled protons, with N being an integer multiple of the number of protons on each identical guest molecule. For example, each HMB molecule contributes 18 hydrogen atoms to the spin system within a particular supercage. These proton spins are in close proximity to other HMB molecules adsorbed within the same supercage, permitting the proton spins to become correlated to one another after a sufficiently long period of excitation.

Multiple-quantum NMR determines the number of homonuclear dipole–dipole coupled spins in a spin network by measuring the response of the coupled spins to radio-frequency (rf) excitation as a function of the excitation time.[18] In this study, the clustering of HMB within NaY supercages has been examined as a function of adsorbate concentration. HMB loadings of 5.1, 10.2, and 20.4 wt % were used, corresponding to bulk averages of approximately one-half, one, and two HMB molecules per NaY supercage, respectively. As shown for 20.4 wt % HMB/NaY in Figure 9a–c, higher order multiple-quantum intensities increase with lengthening rf excitation times as more spins coherently interact through their dipole couplings. Weaker dipolar couplings become effective at longer excitation times, until ultimately all of the spins within a cluster are interacting with one another. In a zeolite, a natural limit exists on the size of a dipolar-coupled spin system due to physical isolation of the adsorbate molecules in different cavities. As the excitation time is increased under such circumstances, n-quantum peak intensities approach constant values with respect to the total signal intensity (Figure 9d–f), reflecting the limited spin network size of the isolated guest species.

Multiple-Quantum Data Analysis

The number of adsorbed guest molecules within the NaY

(30) Kärger, J.; Pfeifer, H. *Zeolites* **1987**, *7*, 90.
(31) Pickett, S. D.; Nowak, A. K.; Thomas, J. M.; Peterson, B. K.; Swift, J. F. P.; Cheetham, A. K.; den Ouden, C. J. J.; Smit, B.; Post, M. F. M. *J. Phys. Chem.* **1990**, *94*, 1233.
(32) Ryoo, R.; Pak, C.; Chmelka, B. F. *Zeolites*, in press.

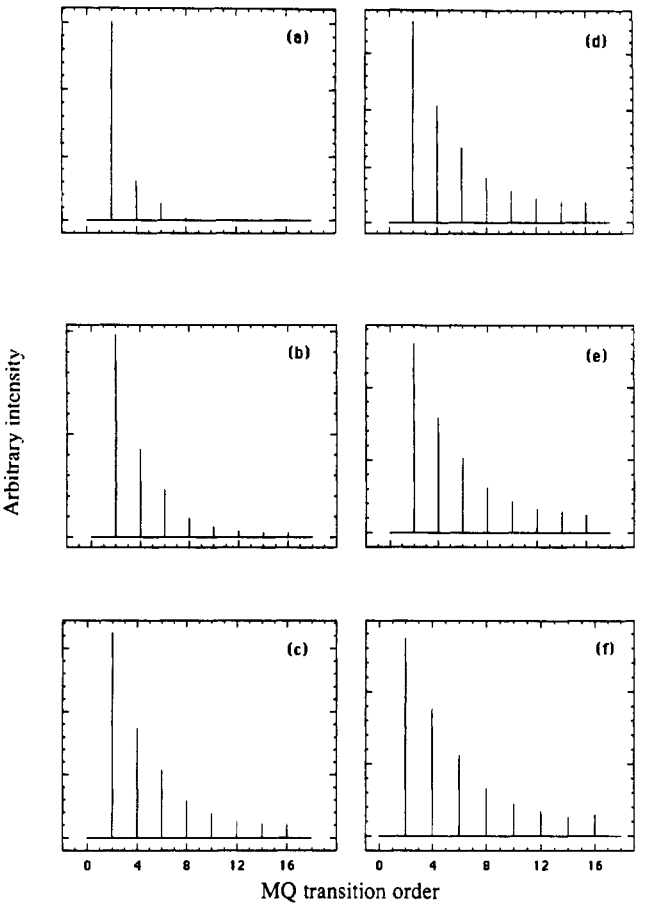

Figure 9. Proton multiple-quantum NMR spectra of 20.4 wt % HMB adsorbed at 573 K on dehydrated NaY zeolite. The spectra were acquired at different radio-frequency excitation times: (a) 132, (b) 264, (c) 396, (d) 528, (e) 660, and (f) 792 μs.

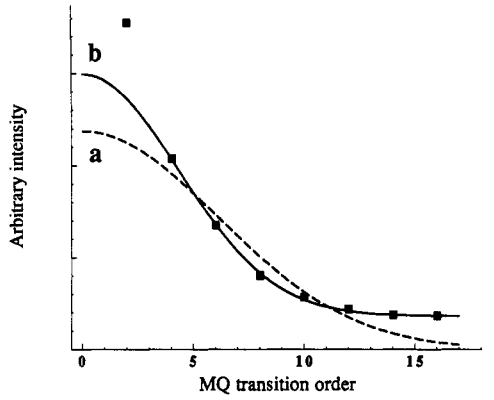

Figure 10. Gaussian fits to the proton multiple-quantum NMR data of Figure 9d for 20.4 wt % HMB adsorbed at 573 K on dehydrated NaY zeolite. Each point represents the measured n-quantum peak intensity associated with a particular n-quantum transition. The data were acquired with a radio-frequency excitation time of 528 μs.

cavities can be determined by measuring the size of a spin system using multiple-quantum NMR. For a given excitation time, the resulting MQ spectrum (e.g., Figure 9), can be fit in the statistical limit to a Gaussian curve with a standard deviation of $(N/2)^{1/2}$, where N is the spin network size.[22] We observe for protons on adsorbed molecules that the two-quantum signal decays more slowly than the intensities of higher order transitions.[20] This may be due to a fraction of the proton clusters that have not evolved yet to the maximum spin network limit. Similar behavior is seen in multiple-quantum simulations and studies of nematic liquid crystals prior to reaching the statistical limit.[17] The two-quantum peak in the multiple-quantum spectra of adsorbed HMB is consequently more intense than that predicted by the Gaussian model

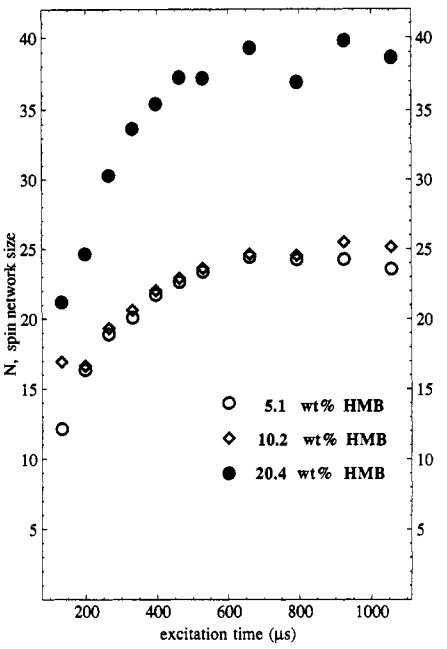

Figure 11. Results of proton multiple-quantum NMR experiments for HMB adsorbed at 573 K on dehydrated NaY zeolite.

derived from statistical arguments.[22]

Neglecting the two-quantum transition, Figure 10a displays the Gaussian fit to the multiple-quantum results for 20.4 wt % HMB in NaY. The discrepancy between curve a and the data is still appreciable, because finite MQ peak intensities exist for higher order transitions. This solid-lattice-like behavior can probably be attributed to a small amount of residual, unadsorbed solid HMB located in the pore spaces between the micron-sized crystallites. A baseline correction effectively eliminates the contribution of bulk HMB to the multiple-quantum signal by recalibrating the intensity scale to zero at the highest transition orders. Curve b is a baseline-corrected Gaussian fit that demonstrates good agreement with the data.

If the resulting spin network size N is plotted as a function of radio-frequency excitation time, cluster sizes for various macroscopically uniform adsorbate loadings can be determined. For NaY samples containing 5.1 and 10.2 wt % HMB, the Gaussian-fit values for N in Figure 11 approach maximum spin network sizes N_{max} of about 23 and 24 spins, respectively. The nearly overlapping MQ data for these samples suggest similar spin clustering behavior and, thus, similar local distribution of adsorbed HMB guest species. Statistical dispersion of the HMB guests would produce higher incidences of double and triple HMB–supercage occupancies (Figure 8a), manifested by a markedly higher maximum spin network size, in the 10.2 wt % HMB/NaY sample compared to the 5.1 wt % HMB/NaY material. Because the two loadings display nearly identical spin coupling behavior in response to multiple-quantum excitation, the distribution of HMB guest species in NaY at 573 K cannot be statistical. Moreover, values of $N_{max} \approx 23$ or 24 compare favorably with the number of protons on a single molecule of HMB (18 hydrogen atoms), indicating a local distribution of about one HMB molecule per supercage cavity. This is consistent with homogeneous dispersal of HMB molecules throughout the NaY crystallite matrix. At HMB loadings above 10.2 wt %, the supercages accept a second adsorbed guest molecule. For 20.4 wt % HMB/NaY, the limiting cluster size is measured to be $N_{max} \approx 38$, reflecting an occupancy of two HMB guests per supercage. The MQ data of Figure 11 show the HMB guests to be dispersed in an essentially homogeneous manner throughout the NaY matrix, as depicted in Figure 8b.

Conclusions

From our ^{129}Xe NMR investigation, it is clear that extensive thermal treatment is required to disperse guest molecules adsorbed in the supercage cavities throughout a macroscopic sample volume.

Room-temperature ^{129}Xe NMR is a convenient means of studying heterogeneous distributions of HMB in NaY, providing the heterogeneity length scales are larger than about 10 μm. Such situations may lend themselves to NMR chemical shift imaging methods in which a linear magnetic field gradient might be used to image xenon profiles in samples possessing macroscopic adsorbate heterogeneities. The suitability of multiple-quantum NMR spectroscopy for probing adsorbate distributions quantitatively is due primarily to the sensitivity of the technique to the number of dipole–dipole coupled spins in a collection of isolated molecules. Counting the number of proton spins in clusters of chemisorbed organic species yields information on their spatial distributions and, thus, about microstructural features of the adsorption sites themselves. Because of the central importance of these sites to the reaction process, multiple-quantum NMR represents a potentially valuable means by which a catalyst's microscopic adsorbate structure can be correlated with its chemical reaction properties. Such information, used in conjunction with the macroscopic adsorbate distributions measured by ^{129}Xe NMR spectroscopy, is key to characterizing intracrystalline mass transport and adsorption of reactant species within zeolitic catalysts.

Acknowledgment. We thank D. N. Shykind and M. Trecoske for assistance with the multiple-quantum experiments and with zeolite sample preparation. M. G. Samant kindly provided the NaY zeolite used. This work was supported by the Director, Office of Energy Research, Office of Basic Energy Sciences, Materials Sciences Division of the U.S. Department of Energy, under Contract No. DE-AC03-76SF00098.

Preparation and Characterization of Highly Dispersed Cobalt Oxide and Sulfide Catalysts Supported on SiO_2

Yasuaki Okamoto,*,† Kozo Nagata,† Toshinori Adachi,† Toshinobu Imanaka,† Kazuhiro Inamura,‡ and Toshiyuki Takyu‡

Department of Chemical Engineering, Faculty of Engineering Science, Osaka University, Toyonaka, Osaka 560, Japan, and Central Research Laboratories, Idemitsu Kosan Co., Ltd., 1280, Kamiizumi, Sodegaura-machi, Kimitsu-gun, Chiba 299-02, Japan *(Received: June 13, 1990)*

Physicochemical characterization of calcined and sulfided CoO/SiO_2 catalysts were carried out to reveal the interaction modes between cobalt and SiO_2 using XPS, TPR, TEM, DRS-VIS, and XRD techniques. The CoO/SiO_2 catalysts were prepared by an impregnation method using cobalt acetate as well as cobalt nitrate and by an ion-exchange technique. It was found that several kinds of cobalt species are formed on CoO/SiO_2. These species are assigned to Co_3O_4, Co–Si–O mixed oxide, surface Co^{3+} species, surface silicate, surface Co^{2+} species in the order of the TPR reduction temperature. Their proportions strongly depended on the starting salt, cobalt content, and preparation method. Cobalt acetate was found to provide highly dispersed CoO/SiO_2 catalysts with a uniform distribution of cobalt species throughout the catalyst particles as compared to conventionally employed cobalt nitrate. The proportion of Co^{3+} greatly decreased when cobalt acetate was used instead of cobalt nitrate. All the cobalt species interacting with SiO_2 were found to be sulfided at 673 K. It was demonstrated that sulfided CoO/SiO_2 catalysts prepared from cobalt acetate show several times higher hydrogenation activity than the catalysts from cobalt nitrate. On the basis of the XPS characterization of uncalcined precursors, the effects of starting salt on the cobalt–SiO_2 interaction modes and cobalt dispersion and distribution are discussed.

Introduction

Supported cobalt–molybdenum sulfide catalysts have been widely employed for hydroprocessing of petroleum feedstocks and extensively investigated by many workers.[1,2] Recently, Topsøe et al.[3,4] have proposed that the formation of so-called Co–Mo–S phases generate catalytic synergies between Co and Mo. The Co sites in the Co–Mo–S phases are considered to form catalytically active centers. In addition, de Beer and Prins et al.[5-8] have shown that carbon-supported cobalt sulfides exhibit very high hydrodesulfurization (HDS) activities as compared to carbon- or alumina-supported molybdenum sulfide catalysts, suggesting that sulfided cobalt species show a high HDS activity in a specific configuration as the Co species in the Co–Mo–S phases do. Besides hydrotreating processes, supported cobalt metal catalysts are extensively used for the hydrogenation of carbon monoxide to produce hydrocarbons.[9,10]

The physicochemical characterization of Al_2O_3-supported cobalt catalysts has shown the presence of several cobalt species in oxide states by using XPS,[11-16] X-ray absorption spectroscopy (XAS),[17] temperature-programmed reduction (TPR),[18,19] and other techniques.[20-23] Detailed characterization of cobalt species on SiO_2-supported catalysts are, however, very scarce as compared with CoO/Al_2O_3 systems. Very recently, Castner et al.[24,25] have shown by using TPR, XPS, AEM, XAS, and XRD that after

† Osaka University.
‡ Idemitsu Kosan Co.

(1) Massoth, F. E. *Adv. Catal.* **1978**, *27*, 265.
(2) Grange, P. *Catal. Rev.-Sci. Eng.* **1980**, *21*, 135.
(3) Topsøe, H.; Clausen, B. S. *Catal. Rev.-Sci. Eng.* **1984**, *26*, 395.
(4) Wievel, C.; Candia, R.; Clausen, B. S.; Morøp, S.; Topsøe, H. *J. Catal.* **1981**, *68*, 453.
(5) Prins, R.; de Beer, V. H. J.; Somorjai, G. A. *Catal. Rev.-Sci. Eng.* **1989**, *31*, 1.
(6) Vissers, J. P. R.; de Beer, V. H. J.; Prins, R. *J. Chem. Soc., Faraday Trans. 1* **1987**, *83*, 2145.
(7) Duchet, J. C.; van Oers, E. M.; de Beer, V. H. J.; Prins, R. *J. Catal.* **1983**, *80*, 386.
(8) Bouwens, S. M. A. M.; Koningsberger, D. C.; de Beer, V. H. J.; Prins, R. *Catal. Lett.* **1988**, *1*, 55.
(9) Vannice, M. A.; Garten, R. L. *J. Catal.* **1979**, *56*, 236.
(10) Anderson, R. B. *The Fischer–Tropsch Synthesis*; Academic Press: New York, 1984.
(11) Okamoto, Y.; Nakano, H.; Imanaka, I.; Teranishi, S. *Bull. Chem. Soc. Jpn.* **1975**, *48*, 1163.
(12) Okamoto, Y.; Imanaka, I.; Teranishi, S. *J. Catal.* **1980**, *65*, 448.
(13) Grimblot, J.; Bonnelle, J. P.; Beaufils, J. P. *J. Electron Spectrosc. Relat. Phenom.* **1976**, *8*, 437.
(14) Bonnelle, J. P.; Grimblot, J.; D'Huysser, A. *J. Electron Spectrosc. Relat. Phenom.* **1975**, *7*, 151.
(15) Declerck-Grimee, R. I.; Canesson, P.; Friedman, R. M.; Fripiat, J. J. *J. Phys. Chem.* **1978**, *82*, 885.
(16) Chin, R. L.; Hercules, D. M. *J. Phys. Chem.* **1982**, *86*, 360.

0022-3654/91/2095-0310$02.50/0